Bias-free, low power and optically driven membrane InP switch on SOI for remotely configurable photonic packet switches

M. Tassaert,[1,*] G. Roelkens,[1] H. J. S. Dorren,[2] D. Van Thourhout,[1] and O. Raz[2]

[1]*Photonics Research Group - Ghent University/imec, Sint-Pietersnieuwstraat 41, 9000 Gent, Belgium*

[2]*Eindhoven University of Technology, Den Dolech 2, 5600MB, Eindhoven, The Netherlands*

[*]*martijn.tassaert@intec.ugent.be*

Abstract: A small footprint integrated Membrane InP Switch (MIPS) on Silicon-On-Insulator (SOI) is demonstrated for use in all-optical packet switching. The device consists of an optically pumped III-V membrane waveguide of only 100 nm thick, coupled to the underlying SOI waveguide circuit. Because of its limited thickness, the optical confinement in the active layers is maximized, allowing for high extinction ratio of over 30 dB when applying a low power optical pump signal, over the entire C-band. The switch has 400/1300 ps on/off switching times and no measurable pattern dependence or switching related power penalties for a bitrate up to 40 Gb/s, using a switching power of only 2 dBm.

OCIS codes: (130.0130) Integrated optics; (130.4815) Optical switching devices; (060.6719) Switching, packet.

References and links

1. www.cisco.com/en/US/docs/routers/crs/hardware_doc/roadmap/17014hdg.html.
2. S. J. Ben Yoo, "Optical packet and burst switching technologies for the future photonic Internet," J. Lightwave Technol. **24**, 4468–4492 (2006).
3. R. S. Tucker, "Scalability and energy consumption of optical and electronic packet switching," J. Lightwave Technol. **29**, 1–12 (2011).
4. I. M. Soganci, T. Tanemura, K. A. Williams, N. Calabretta, T. De Vries, E. Smalbrugge, M. K. Smit, H. Dorren, and Y. Nakano, "Monolithically integrated InP 1x16 optical switch with wavelength-insensitive operation," IEEE Photon. Technol. Lett. **22**, 143–145 (2010).
5. A. Albores-Mejia, F. Gomez-Agis, H. J. S. Dorren, X. J. M. Leijtens, T. de Vries, Y.-S. Oei, M. J. R. Heck, R. Notzel, D. J. Robbins, M. K. Smit, and K. A. Williams, "Monolithic multistage optoelectronic switch circuit routing 160 Gb/s line-rate data," J. Lightwave Technol. **28**, 2984–2992 (2010).
6. A. Bianco, D. Cuda, R. Gaudino, G. Gavilanes, F. Neri, and M. Petracca, "Scalability of optical interconnects based on microring resonators," IEEE Photon. Technol. Lett. **22**, 1081–1083 (2010).
7. N. Calabretta, H. Jung, J. Lorente, E. Tangdiongga, T. Koonen, and H. Dorren, "All-optical techniques enabling packet switching with label processing and label rewriting," J. Telecommun. Inf. Technol., 20–28 (2009).
8. J. E. Sharping, M. Fiorentino, P. Kumar, and R. S. Windeler, "All-optical switching based on cross-phase modulation in microstructure fiber," IEEE Photon. Technol. Let. **14**, 77–79 (2002).
9. W. Bogaerts, L. Liu, S. Selvaraja, J. Brouckaert, D. Taillaert, D. Vermeulen, G. Roelkens, D. Van Thourhout, and R. Baets, "Silicon nanophotonic waveguides and their applications," Proc. SPIE **7134**, 71341O (2008).
10. G. Roelkens, J. Brouckaert, D. Van Thourhout, R. Baets, R. Notzel, and M. Smit, "Adhesive bonding of InP/InGaAsP dies to processed silicon-on-insulator wafers using dvs-bis-benzocyclobutene," J. Electrochem. Soc. **153**, G1015–G1019 (2006).

#157156 - $15.00 USD Received 1 Nov 2011; revised 30 Nov 2011; accepted 1 Dec 2011; published 6 Dec 2011

11. G. Roelkens, L. Liu, D. Liang, R. Jones, A. Fang, B. Koch, and J. Bowers, "III-V/silicon photonics for on-chip and inter-chip optical interconnects," Laser Photon. Rev. **4**, 751–779 (2010).
12. M. Tassaert, S. Keyvaninia, D. Van Thourhout, W. M. J. Green, Y. Vlasov, and G. Roelkens, "A nanophotonic InP/InGaAlAs optical amplifier integrated on a silicon-on-insulator waveguide circuit," in *Proceedings of IEEE Conference on Information Photonics* (Institute of Electrical and Electronics Engineers, Ottawa, 2011), pp. 1-2.
13. D. Taillaert, F. Van Laere, M. Ayre, W. Bogaerts, D. Van Thourhout, P. Bienstman, and R. Baets, "Grating couplers for coupling between optical fibers and nanophotonic waveguides," Jpn. J. Appl. Phys. Part 1-Regul. Pap. Brief Commun. **45**, 6071–6077 (2006).
14. www.epixfab.eu.
15. F. Doany, B. Lee, S. Assefa, W. Green, M. Yang, C. Schow, C. Jahnes, S. Zhang, J. Singer, V. Kopp, J. Kash, and Y. Vlasov, "Multichannel high-bandwidth coupling of ultra-dense silicon photonic waveguide array to standard-pitch fiber array," J. Lightwave Technol. **29**, 475–482 (2011).

1. Introduction

Since the beginning of the "Internet Age", the number of connected hosts and used bandwidth have been growing exponentially. This trend is still continuing with the onset of bandwidth demanding services as video-on-demand and cloud computing. Most of this data is sent using the Internet Protocol (IP) which bundles the data in small packets each containing a header with an address, so that each packet can find its way to the right destination. In each node where several optical channels meet, a routing system converts the optically transmitted data to the electrical domain where the address information is read, deciphered and the data packet is routed along the right optical link. Due to the continuing increase in transmitted data, these systems are growing in both floor space and power consumption [1]. Much of this growth can be attributed to the large amount of power and space needed for the forwarding engines which include the conversion of optical packets to the electrical domain and back again. This is the reason why a large research effort has been put into building an all-optical packet switch that could replace its electrical counterpart in recent years.

Both pure all-optical and hybrid electro-optic solutions have been investigated [2, 3]. On the hybrid front, various switch architectures have been investigated which either use electrically driven phase shifters [4], semiconductor optical amplifiers (SOAs) [5] or microring resonators [6]. Effort has also been put into building all-optical systems. In these demonstrations the phase or resonance condition of a device was changed by an external optical signal to obtain switching of the data signal. There have been demonstrations using electrically biased integrated devices based on Mach Zehnder Interferometers (MZIs) and SOAs [7] and unbiased fiber based switches which are using fiber non-linearities for the switching operation and therefore require very high optical powers [8]. Although these solutions are all-optical, their power consumption is still comparable to state-of-the-art electrical switching, with a significant contribution due to driving circuits, electrical bias and operating power of the individual switching components [3].

The integration of an all-optical switch made in a bonded III-V membrane layer on top of the SOI waveguide platform would allow for the creation of more complex circuits, including active and passive devices, which are necessary for the realization of complex packet switches [9]. Integration of the III-V membrane can be achieved via adhesive die-to-wafer bonding using DVS-BCB as an intermediate adhesive [10]. Using this integration method several electrically pumped lasers and amplifiers have already been demonstrated [11]. In these approaches, the active III-V waveguide is at least 500 nm thick, to ensure efficient electrical pumping of the device. This limits the maximal confinement one can achieve in the active layers, increasing the required device's length to achieve a sufficiently high extinction ratio (ER) and therefore also the power consumption. If only optical excitation of the gain medium were used however, current injection layers and ohmic contacts would no longer be required, reducing the required III-V waveguide thickness. As a result, this allows for the use of the high index contrast be-

#157156 - $15.00 USD Received 1 Nov 2011; revised 30 Nov 2011; accepted 1 Dec 2011; published 6 Dec 2011

tween the III-V layers and the surrounding DVS-BCB cladding layer to create III-V membrane waveguides which have a much higher confinement in the active layers.

In this article, we propose to use an optically pumped ultra-thin (<100 nm) Membrane InP Switch (MIPS) within a broadcast-and-select switching architecture on the SOI waveguide platform as a complementary device in the heterogeneous integration tool box to solve many of the issues hindering the adaptation of all-optical packet switches. In this demonstration we highlight the switching performance of a single MIPS device which can be optically driven using a low power switching signal (<2 mW) between high absorption and transparency with more than 30 dB extinction ratio and rise and fall times measuring 400 and 1300 ps respectively. Switching of 20 and 40 Gb/s NRZ-OOK data packets was accomplished with the switch showing no pattern dependence or any power penalty related to the switch operation.

The paper is arranged as follows. In section 2 we introduce the general switch architecture which will make use of the MIPS. Section 3 is devoted to the device layout and fabrication. Section 4 gives static and dynamic switching characterization results while section 5 gives first experimental results of the operation of the MIPS in the context of all-optical packet switching. We conclude the paper in section 6 with some discussion and conclusions.

2. Switching architecture

In Fig. 1 the proposed switch architecture is schematically shown for a $1\times m$ packet switch. It is a common broadcast-and-select architecture, with a MIPS as the switching element. To drive the switches all-optically, a scheme is proposed in which the label processor extracts the out-of-band labels, filters them using an Arrayed Waveguide Grating (AWG) and then recombines them using a MZI, with one of the m copies of the data packet at the input of one of the m switches. By using m of these blocks, a $m\times m$ packet switch can be made [3]. Note that the label extraction can be done at a remote location, as the generated labels are low-power optical signals.

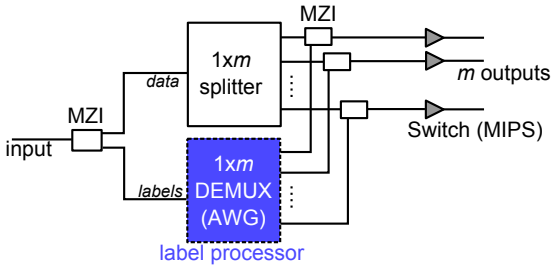

Fig. 1. Proposed packet switch architecture of a $1\times m$ switch.

3. Device layout and fabrication

The device layout is schematically shown in Fig. 2(a). It consists of a 100 nm thick III-V membrane waveguide which is coupled to two underlying silicon access waveguides using two inverted taper couplers. In such an inverted taper coupler, a 220 nm thick silicon waveguide tapers linearly over a length of 18 μm from a starting width of 700 nm down to a width of 100 nm, while the III-V membrane waveguide on top tapers linearly from a width of 0.5 μm to a width of 1.4 μm. The coupler is designed to allow an adiabatic transition from the fundamental TE-mode in the silicon waveguide to the fundamental TE-mode in the III-V membrane waveguide.

The III-V waveguide has the structure of a rib waveguide with a width of 1.4 μm. It is made by shallow etching a bonded III-V epitaxial layer stack, which consists of three 8 nm thick

#157156 - $15.00 USD Received 1 Nov 2011; revised 30 Nov 2011; accepted 1 Dec 2011; published 6 Dec 2011

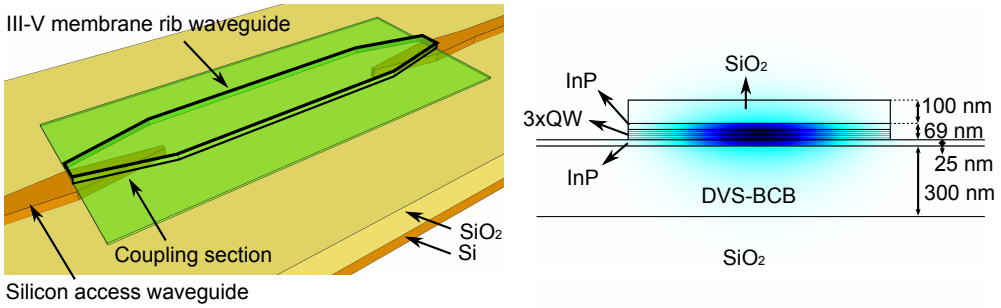

Fig. 2. (a) Schematic view of the device. It consists of two access waveguides, which are coupled to a III-V membrane waveguide using two inverted taper couplers. (b) The mode profile in the III-V membrane waveguide. The high intensity in the quantum well layers is clearly visible.

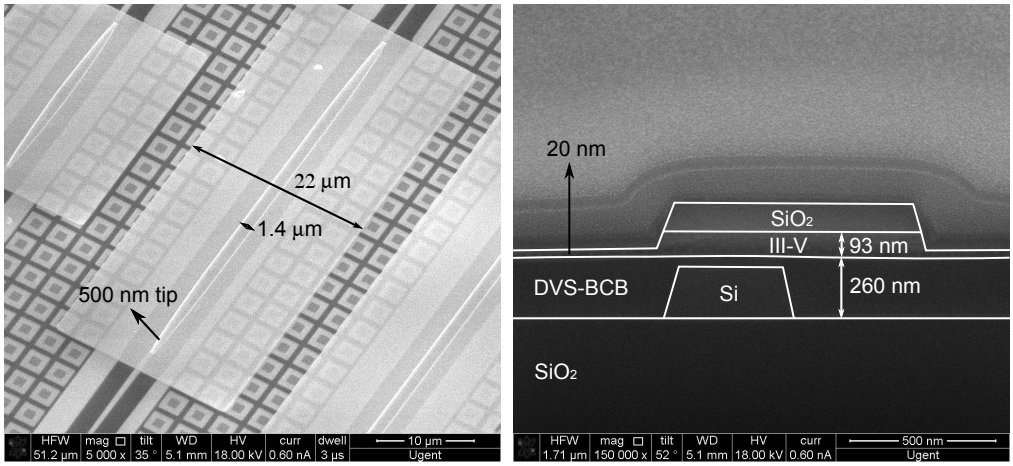

Fig. 3. (a) An SEM image of a 50 μm and a 100 μm long device. (b) SEM image of a cross section through the tapered part.

InGaAs quantum wells, separated by 10 nm thick InP barrier layers. This quantum well stack is sandwiched between two 25 nm thick InP cladding layers. The band gap wavelength for this configuration was determined to be 1.58 μm. A rib waveguide structure is favored over a strip waveguide because the shallow etched cladding layers form a path along which dissipated heat can escape, significantly reducing the thermal resistance of the device [12]. The mode profile in the III-V rib waveguide is shown in Fig. 2(b) for a remaining cladding thickness of 25 nm. The high intensity in the quantum well layers is clearly visible and a confinement of 0.17 is reached in the active layers. Thanks to this very high confinement, a high ER is possible with a short device length. Furthermore, as only three quantum wells are used, the device can be saturated using a low pump power. The device is coupled to optical input/output fibers through two grating couplers, which show a coupling loss of 6.5 dB per coupler at a peak wavelength of 1530 nm and a 3 dB bandwidth of 70 nm [13].

Fabrication of the SOI waveguide circuits was done using a 193 nm deep UV lithography stepper and dry etching on a 200 mm wafer in a CMOS pilot-line [14]. After dicing of the SOI

#157156 - $15.00 USD Received 1 Nov 2011; revised 30 Nov 2011; accepted 1 Dec 2011; published 6 Dec 2011

wafer, the seperate dies are cleaned in a standard clean-1 solution for 15 minutes. In the mean time, the III-V dies are prepared for bonding by removal of the InP/InGaAs sacrificial layer pair, using HCl and a $1H_2SO_4$:$1H_2O_2$:$18H_2O$ solution respectively. To improve adhesion to the DVS-BCB adhesive layer, a thin layer of 10 nm of SiO_2 is deposited on the III-V dies. After this, a DVS-BCB solution diluted with mesitylene (5BCB:9Mes) is spincoated on the SOI dies. After evaporation of the mesitylene, the dies are brought into close contact in a controlled environment using a bonding pressure of 1.25 MPa and cured for one hour at 240C. After the bonding of the dies, the InP substrate is removed using a combination of mechanical grinding and chemical etching using HCl until the InGaAs etch stop layer is reached. Subsequently the etch stop layer is removed using a $1H_2SO_4$:$1H_2O_2$:$18H_2O$ solution and a 100 nm thick SiO_2 hard mask is deposited. This hard mask is patterned using contact lithography to create the core of the rib waveguide. After dry etching the hard mask, the bonded III-V film is etched until 20 nm remains in the etched parts. Afterwards, another contact lithography step is performed to define the III-V islands and the remaining 20 nm is etched using a $NaClO_3$:HCl:CH_3COOH:H_2O solution, which is an isotropic etch mixture for InP and InGaAs. In Fig. 3(a) a Scanning Electron Microscopy (SEM) image of the resulting devices is shown and in Fig. 3(b) a SEM image of the cross section through one of the taper structures is shown. From this image it can be seen that the DVS-BCB bonding layer thickness is 260 nm in the trenches of the 220 nm thick silicon waveguides, leading to a thickness of only 40 nm between the two coupled waveguides. The two structures were misaligned by 200 nm which is within the margin to have good coupling.

4. Device characterization

4.1. Extinction ratio

To determine the maximal ER our MIPS can deliver, we performed a continuous wave (CW) pump-probe experiment. In this experiment a CW pump beam at 1505 nm was combined with a CW probe beam using a 99/1 combiner and sent through the device. By comparing the probe transmission to the transmission through a reference silicon waveguide, the device absorption

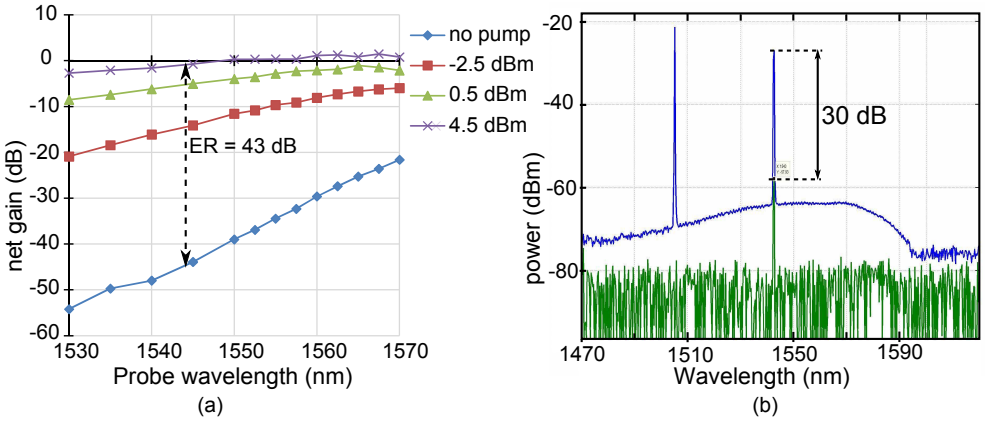

Fig. 4. (a) Measured net gain for the CW pump-probe experiment. The different curves correspond to a different pump power, while the probe wavelength is varied along the x-axis. The displayed pump power is the on-chip pump power, which was calculated by subtracting a measured 7.5 dB coupling loss for the pump wavelength from the measured pump power before coupling to the chip. The pump wavelength was everywhere 1505 nm. (b) Optical spectra at the output of the device showing the achieved extinction ratio for a pump power of -2 dBm.

#157156 - $15.00 USD Received 1 Nov 2011; revised 30 Nov 2011; accepted 1 Dec 2011; published 6 Dec 2011

and gain can be determined. To avoid self-saturating effects by the probe beam, the on-chip input probe power was set as low as −19 dBm. By varying the probe wavelength and the pump power, the ER can be extracted as a function of wavelength and power consumption. To derive the on-chip pump power, the grating coupler efficiency was estimated using the transmission measurement through the reference waveguide. The results for a 150 μm long device are shown in Fig. 4. When the pump power is increased, more photons are absorbed and therefore more free carriers are generated. Because of these free carriers the absorption of the probe beam will decrease and eventually a net gain of 2 dB is reached. For higher powers however, the net gain does not increase further. The cause for this low gain lies with thermal effects [12], which smoothen the Fermi-Dirac distribution of the generated carriers. Next to directly reducing the gain, this also reduces the absorption of the pump beam. Consequently less carriers are generated for a certain pump power. This effect can be observed when looking at the net gain curves for short wavelengths in Fig. 4(a). Therefore, improving the thermal design of the device by adding a heat spreader should lead to higher gains. Also moving to a more broadband fiber-to-chip coupling scheme so that pumping at shorter wavelengths is made possible could improve the performance.

Due to the fact that the probe beam absorption is bleached by the pump beam, a high ER can be achieved (Fig. 4(b)). Comparing the net gain curve without pump with a net gain curve with applied pump yields the ER for the device, assuming that the steady state is reached. This leads to an ER of over 30 dB over the entire C-band for a pump power of 4.5 dBm.

4.2. Switching speed

To be able to serve as an all-optical packet switch, the device needs to switch fast enough between the steady state situations with and without pump. Therefore, the switch on/switch off times of the device were measured by applying a realistic switching signal at a wavelength of 1505 nm, which is on during a period of 195 ns and off during a switching window of 5 ns. By monitoring the resulting modulation of an injected CW probe signal at 1542 nm with an optical oscilloscope, the switching times can be extracted. In Fig. 5(a) traces of the rising and falling edge of such a switching window are shown. From this the switch on and the switch off time are determined to be respectively 400 ps and 1.3 ns. Using a switching window of 5 ns, this is more than fast enough to ensure that the achieved ER in the CW experiment is also achieved in a dynamic switching experiment. To demonstrate this, in Fig. 5(b) a trace of a switching window between two switched packets is shown.

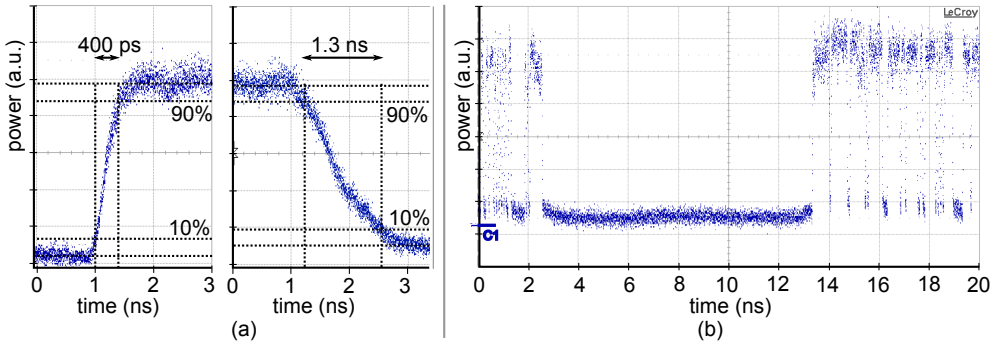

Fig. 5. (a) Traces of a 1545 nm probe signal being switched on and off by a 1505 nm pump. From this, a switch on and switch off time of respectively 400 ps and 1.3 ns can be extracted. (b) Time trace of the switching window between two data packets.

#157156 - $15.00 USD Received 1 Nov 2011; revised 30 Nov 2011; accepted 1 Dec 2011; published 6 Dec 2011

5. Packet switching experiment

To demonstrate the use of the MIPS as a packet switch, we have used the setup as depicted in Fig. 6. The data signal was sent at a wavelength of 1542.5 nm with an average on-chip power of −12 dBm. The pump was set at 1505 nm and an average on-chip power of 2 dBm was used to pump the device. For this pump power, the switch exhibits an ER of over 30 dB and has an insertion loss of 4.5 dB for the data signal due to incomplete bleaching of the device. Together with the grating coupler loss, this leads to a total insertion loss of 19 dB. Two experiments were performed. First, the performance of the switch was characterized under constant pumping and at a data rate of 20 Gbit/s to check for any pattern dependence of the device. In this experiment, different length pseudorandom binary sequences (PRBS) were sent through the device and were compared to a back-to-back measurement. From Fig. 7(a), it is clear that no pattern dependence exists, as the measured bit error rate (BER) curves coincide for both PRBS sequences and that furthermore the switching operation does not lead to a receiver sensitivity penalty. In the second experiment, the pattern generator for the data signal was programmed to give 195/5 ns packets at data rates of both 20 and 40 Gbit/s, while the pump beam was programmed to be switched on

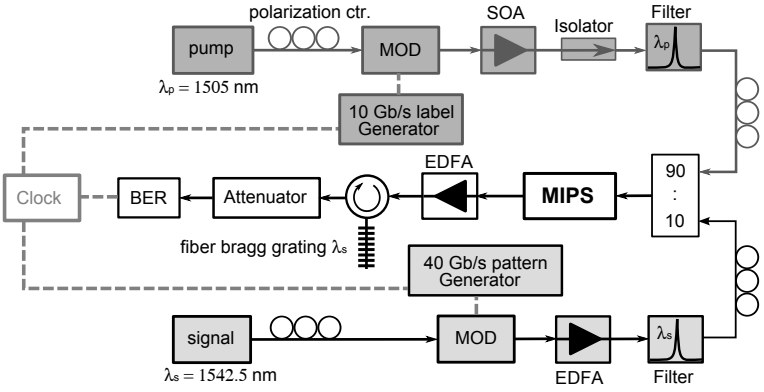

Fig. 6. Setup for the packet switching experiment.

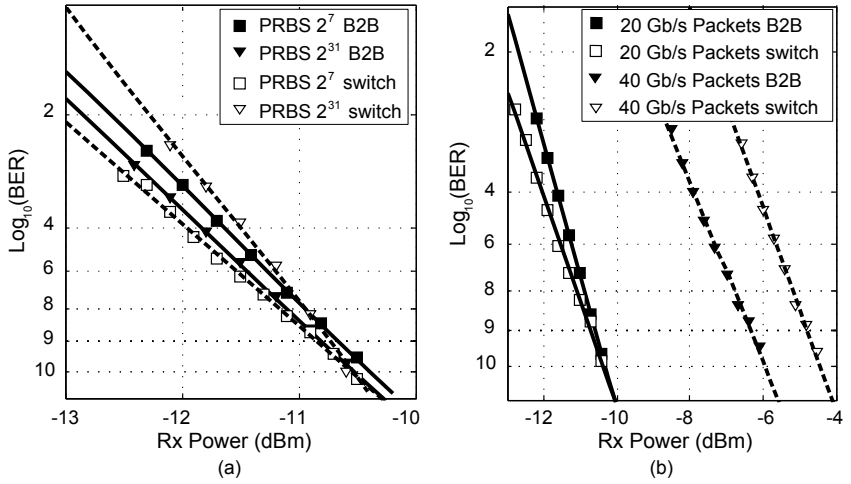

Fig. 7. (a) Measured BER for different PRBS sequences at a bit rate of 20 Gbit/s. (b) Measured BER at 20 Gbit/s and 40 Gbit/s, both back-to-back (B2B) and through the switch.

#157156 - $15.00 USD Received 1 Nov 2011; revised 30 Nov 2011; accepted 1 Dec 2011; published 6 Dec 2011

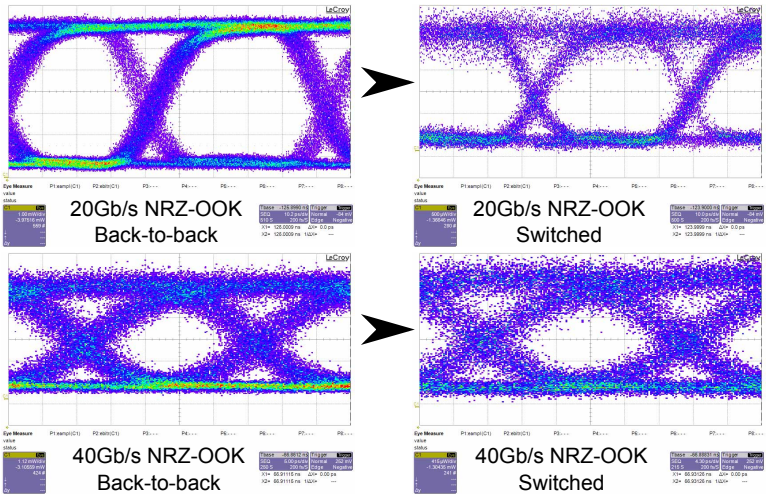

Fig. 8. (Left) Eye patterns obtained by a back-to-back measurement. (Right) Eye patterns obtained after switching. Note the increased noise for both the 20 Gbit/s and the 40 Gbit/s signal in the switching experiment. This noise is associated with the use of an extra EDFA to reach adequate signal power levels in the case of the switching experiment.

during the packet and switched off in between two packets. In Fig. 8 the eye patterns obtained in this experiment can be seen and in Fig. 7(b) the corresponding BER curves are plotted. From the BER curves, it is clear that there is no receiver sensitivity penalty due to the switching operation for the 20 Gbit/s signal. However at 40 Gbit/s, a penalty of 1.5 dB is observed. This penalty is associated with the limited output power at the output grating coupler, which requires the use of an EDFA to amplify the signal. This degrades the optical signal to noise ratio, as can be seen in the eye diagrams for both 20 Gbit/s and 40 Gbit/s signals, but because of a high ER in the 20 Gbit/s signal a receiver sensitivity penalty is only observed at 40 Gbit/s.

6. Conclusion

We have proposed and characterized a novel all-optical membrane InP switch (MIPS) integrated on SOI, based on an ultra-thin bonded III-V membrane waveguide. Using this device a net gain of up to 2 dB has been measured and an ER of over 30 dB over the entire C-band was demonstrated for a pump power of 4.5 dBm. The device's switch on and switch off times were determined to be 400 ps and 1.3 ns respectively, fast enough to do all-optical packet switching. Finally, we demonstrated penalty free all-optical switching of 20 and 40 Gbit/s packets using a very low on-chip pumping power of 2 dBm. In future designs, a $1\times m$ switch will be made, using the proposed broadcast-and-select architecture which uses the MIPS as key switching component. Furthermore, a more broadband and efficient fiber-to-chip coupling scheme using horizontal coupling to a SU8 polymer waveguide on SOI will be used, to avoid the high grating coupling losses and allow for lower pump wavelengths to be used. Using the method proposed in [15], the coupling loss can even be brought down to 0.5 dB. Additionally, by narrowing down the MIPS waveguide, the quantum well volume and therefore power consumption can be reduced while having only a minimal impact on the achieved confinement. These measures should allow for the use of a directly modulated laser as a pump signal.

#157156 - $15.00 USD Received 1 Nov 2011; revised 30 Nov 2011; accepted 1 Dec 2011; published 6 Dec 2011